

## NON-ISOTHERMAL STUDIES ON CRYSTALLIZATION KINETICS OF TELLURITE 20Li<sub>2</sub>O-80TeO<sub>2</sub> GLASS

E. B. Araújo\* and E. Idalgo

Universidade Estadual Paulista (Unesp), Departamento de Física e Química, Caixa Postal 31, 15385-000 Ilha Solteira, SP, Brazil

Structural and thermal properties of the 20Li<sub>2</sub>O-80TeO<sub>2</sub> glass were studied using X-ray diffraction analysis and differential scanning calorimetry techniques to understand and control the crystallization process on this glass. The  $\gamma$ -TeO<sub>2</sub>,  $\alpha$ -TeO<sub>2</sub> and  $\alpha$ -Li<sub>2</sub>Te<sub>2</sub>O<sub>5</sub> phases were identified during the crystallization in this glass. Activation energies and Avrami exponent  $n$  were calculated from non-isothermal measurements for glasses with different particle size. The mean values  $\bar{n}$  of Avrami exponent were obtained for glasses with 63–75 and 45–63  $\mu\text{m}$  particle sizes such as  $\bar{n}_1 < \bar{n}_2 < \bar{n}_3$ , but glasses with particle size 38–45  $\mu\text{m}$  and smaller than 38  $\mu\text{m}$  presented  $\bar{n}_1 \approx \bar{n}_2 < \bar{n}_3$ .

**Keywords:** crystallization, glass, tellurium

### Introduction

In recent years, TeO<sub>2</sub>-based glasses attract considerable attention from both the fundamental comprehension and optoelectronic devices applications. Depending on the composition, some TeO<sub>2</sub> glasses present very interesting non-linear properties such as a third harmonic ( $\chi^3$ ) generation almost one order larger than some other important oxide glasses [1, 2]. However, the technological applications of these glasses require a profound comprehension of fundamental characteristics such as structural [3, 4], thermal [5], optical [6] and electrical properties [7, 8]. Nowadays, the technological use of tellurium-based glasses is a reality that justifies progressive investigations on optical, structural and electrical properties [9, 10].

Structural and thermal properties of tellurite glasses are important to the correct comprehension of the nucleation and crystal growth mechanisms, which understanding are fundamental to prepare a high quality glass. In some cases, these studies are vital to choice glasses with optimized parameters to be used in various solid-state devices. The structural and thermal studies of TeO<sub>2</sub>-R ( $R=\text{WO}_3$ ,  $\text{MoO}_3$ ,  $\text{ZnO}$ ,  $\text{V}_2\text{O}_5$  and  $\text{ZnCl}_2$ ) glasses has been widely reported in the literature, such as discussed in both review articles by El-Mallawany [11, 12]. In addition, properties of TeO<sub>2</sub>-Li<sub>2</sub>O glasses were also extensively studied in past years to understand different properties of this important glass matrix, including crystallization kinetics [5] and electrical properties [8]. However, knowledge of the nucleation and crystallization dynamics in a glass is essential to predict devitrification in modern materials development. It is important to

recognize the physical and thermal characteristics of interest, if a glass will be used in technology. It was the spirit of the present paper.

The study of crystallization kinetics in glasses has been widely discussed in the literature by using isothermal and non-isothermal methods. Non-isothermal measurements offer some advantages if compared with isothermal studies. In this way, in past years several different crystallization studies were implemented based on differential thermal analysis (DTA) and differential scanning calorimetry (DSC) techniques. The kinetics of crystallization of several glasses has been extensively obtained from these techniques in isothermal mode. However, non-isothermal DSC measurements, using a constant heating rate until the complete crystallization, are usually applied to study the devitrification on different glasses since the rapidity with which this thermo-analytical technique can be performed.

DSC measurements are preferentially performed on powders and consequently, the interpretation of kinetic crystallization in glasses requires caution in order to understand the particle size effects during crystallization. In this work, glasses with different particle sizes were used to better understand the crystallization process of different phases in the glass matrix and quantify their activation energies. The purpose of the present work is to study the structural and thermal properties of the 20Li<sub>2</sub>O-80TeO<sub>2</sub> glass matrix. By using different glass particle size, the X-ray diffraction analysis (XRD) and DSC techniques were used to understand and control the crystallization process on this glass matrix.

\* Author for correspondence: eudes@dfq.feis.unesp.br

## Theoretical background

The crystallization kinetics of isothermal phase change can be formally described by Johnson–Mehl–Avrami (JMA) theory [13–15]. This model predicts that the volume fraction crystallized ( $x$ ) after a time  $t$ , for an isothermal process, can be expressed by the following equation:

$$x=1-\exp[-(kt)^n] \quad (1)$$

where  $n$  is the Avrami's exponent and  $k$  is the reaction rate constant. The Avrami exponent express the order of the reaction, related to the dimensionality of crystal growth, while  $k$  is a constant related to the activation energy, usually expressed by the Arrhenius-type relation:

$$k=k_0\exp(-E/RT) \quad (2)$$

where  $k_0$  is a frequency factor,  $E$  is the apparent activation energy,  $R$  is the ideal gas constant and  $T$  is the temperature. Alternatively, the logarithmic transformation of Eq. (1) leads to:

$$\ln[-\ln(1-x)]=n\ln k+n\ln t \quad (3)$$

From above equation, at a given temperature, the values of  $n$  and  $k$  can be obtained by a linear fitting of  $\ln[-\ln(1-x)]$  vs.  $\ln t$ . As a plot of  $\ln k$  vs.  $1/T$ , for several isothermal temperatures, is also expected to be linear the activation energy  $E$  can thus be determined by isothermal method.

Alternatively, non-isothermal method can be described based on the assumption that crystallization process is formally described by Avrami theory and considering that temperature increases linearly vs. time such as:

$$T=T_0+\phi t \quad (4)$$

where  $T$  is the temperature at time  $t$ ,  $\phi$  is the heating rate and  $T_0$  is the temperature for  $t=0$ . Applying Johnson–Mehl–Avrami equation to the non-isothermal transition of glasses, introducing the dependence of  $k(t)$ , the Eq. (1) can be rewritten as:

$$x=1-\exp\left[-\left(\int_0^t k(t)dt\right)^n\right] \quad (5)$$

The crystallization rate  $(dx/dt)_p$  of a glass reaches its maximum at a certain temperature  $T_p$ , under the following second derivative consideration:

$$\left.\frac{d^2x}{dt^2}\right|_{T=T_p}=0 \quad (6)$$

A common used method to determine the activation energy  $E$  was developed by Kissinger [16], who showed a linear dependence between  $\ln(T_p^2/\phi)$  vs.

$1/T_p$ . However, from Eqs (5) and (6) the following equation can be obtained:

$$\ln(T_p^2/\phi)=E/RT_p+\text{constant} \quad (7)$$

where  $T_p$  is the temperature corresponding to the maximum of the DSC crystallization peak,  $R$  is the gas constant and  $E$  is the activation energy for the crystallization. Naturally, a plot of  $\ln(T_p^2/\phi)$  vs.  $1/T_p$  would be linear and activation energy can be determined from the slope of the plot. Under consideration that in most crystallization reactions  $E/RT_p \gg 1$  and that  $(dx/dt)_p$  values increase as well as the heating rate, Avrami exponent  $n$  could be determined from the experimental values of the crystallization rate  $(dx/dt)_p$  considering the following equation [17, 18]:

$$n=(dx/dt)_p RT_p^2 (0.37\phi E)^{-1} \quad (8)$$

In this equation,  $x$  is the volume fraction which has been crystallized after time  $t$  behind starting crystallization, the subscript  $p$  denotes the magnitude values corresponding to the maximum crystallization rate,  $R$  is the gas constant,  $\phi$  is the DSC heating rate and  $E$  is the activation energy for the crystallization.

## Experimental

The 20Li<sub>2</sub>O–80TeO<sub>2</sub> glass examined in this work was prepared using the conventional melt quenching method starting from commercial powder reagents Li<sub>2</sub>CO<sub>3</sub> (CBMM, 99.9%) and TeO<sub>2</sub> (Alfa Aesar, 99.95%). After mixing in appropriate proportions, using a 15 g batch mass, the powder was melted using a platinum crucible at 1173 K for 30 min in an electric furnace. The melt obtained was then poured into a polished metal mould, pre-heated at 523 K and immediately placed back in the electric furnace. The glass was maintained inside the furnace at this temperature for 12 h and after low cooling of the furnace, it was finally removed at room temperature.

Powdered glasses with particle size 63–75, 45–63, 38–45 and <38 µm were used for studies reported in this work. The structure of the crystallized glasses was analyzed by XRD using CuK<sub>α</sub> radiation in Rigaku Rotaflex RU200B equipment with a rotating anode. Using a TA Instruments – DSC 2920 (temperature accuracy of ±0.1 K), DSC measurements were performed to study the thermal properties of the studied glasses. DSC measurements were carried out using a constant sample mass of 20 mg, in aluminum pans under a flowing (50 cm<sup>3</sup> min<sup>-1</sup>) atmosphere of dry nitrogen, at four heating rates  $\phi$  (2.5, 5.0, 7.5 and 10 K min<sup>-1</sup>).

Activation energy was evaluated considering that observed DSC crystallization peak is a superposi-

tion of three Gaussian functions, associated to three distinct crystallization phases in the glass devitrification. This assumption was supported by XRD results. The activation energies  $E$  were calculated from Eq. (7) and the slopes of the linear fits to the experimental data from a plot of  $\ln(T_p^2 / \phi)$  vs.  $1/T_p$ , considering that observed DSC exothermic crystallization peak is a result of three distinct crystalline phases in the glass. Finally, Avrami exponents  $n$  were determined from experimental data and Eq. (8) for different heating rates and particle sizes.

## Results and discussion

The structure of the  $20\text{Li}_2\text{O}-80\text{TeO}_2$  glasses was initially studied using the XRD technique. Figure 1 shows XRD patterns of the as-quenched  $20\text{Li}_2\text{O}-80\text{TeO}_2$  glass (Fig. 1a) and previously heat annealed at 642 K (Fig. 1a) for 5 min. Figure 1a shows a typical characteristic of amorphous materials. However, XRD pattern in Fig. 1b shows a partially crystallized material characteristic. The indexed peaks in this figure were attributed to  $\alpha\text{-TeO}_2$  (paratellurite),  $\gamma\text{-TeO}_2$  and  $\alpha\text{-Li}_2\text{Te}_2\text{O}_5$  crystalline phases permeating the glass matrix. The crystalline  $\alpha\text{-TeO}_2$  and  $\gamma\text{-TeO}_2$  phases are two polymorphs of tellurium dioxide  $\text{TeO}_2$ , with this last one considered a metastable structure [19, 20]. Both structures are essentially built up from similar basic  $\text{TeO}_4$  units interconnected by the Te–O–Te simple bridges but present small differences. The structure of the  $\alpha\text{-TeO}_2$  are formed by three-dimensional network  $\text{TeO}_4$  units sharing oxygen corners by symmetric Te–O–Te bridges while the  $\gamma\text{-TeO}_2$  structure can be considered as a chain system, where  $\text{TeO}_4$  units are alternatively linked by nearby and high symmetric Te–O–Te bridges [20]. Based on XRD results shown in Fig. 1b, it was not possible to determine if  $\alpha\text{-TeO}_2$ ,  $\gamma\text{-TeO}_2$  and  $\alpha\text{-Li}_2\text{Te}_2\text{O}_5$  phases crystallize simultaneously or

at distinct onset crystallization temperatures. However, on pure  $\text{TeO}_2$  glass reported in the literature, the  $\gamma\text{-TeO}_2$  appears as the first crystalline phase [21].

The cell parameters and  $d$ -spacing of each crystalline phase were calculated using full-matrix least square method. These parameters were calculated considering the observed ( $h k l$ ) peaks in Fig. 1b for the tetragonal phase of the  $\alpha\text{-TeO}_2$  and the orthorhombic phase of both  $\gamma\text{-TeO}_2$  and  $\alpha\text{-Li}_2\text{Te}_2\text{O}_5$  structures. The calculated and observed parameters were summarized in Table 1 for these crystalline phases. The calculated tetragonal cell parameters  $a=4.801(6)$  Å and  $c=7.616(0)$  Å for the  $\alpha\text{-TeO}_2$  phase are in good agreement with those values reported in the literature for  $\alpha\text{-TeO}_2$  single crystal [19]. In the same manner, the cell parameters of the  $\gamma\text{-TeO}_2$  phase were calculated to obtain  $a=4.805(8)$  Å,  $b=8.785(3)$  Å and  $c=4.344(7)$  Å. These results lead to a structure with a volume cell at around  $183.43$  Å<sup>3</sup>, slightly greater than volume cell ( $182.76$  Å<sup>3</sup>) reported in the literature for the  $\gamma\text{-TeO}_2$  [20]. Finally, the calculated  $a=24.509(6)$  Å,  $b=8.258(2)$  Å and  $c=5.209(3)$  Å cell parameters for  $\alpha\text{-Li}_2\text{Te}_2\text{O}_5$  agrees with results reported in the JCPDS 25-1381 data card.

Figure 2 shows DSC crystallization peaks as a function of the temperature, recorded at different heating rates ( $\phi$ ) and different particle sizes. The top insets in this figure illustrate how the onset glass transition temperature ( $T_g$ ) and the onset crystallization temperature ( $T_x$ ) were determined. In accordance with XRD results, the asymmetry on DSC crystallization peaks suggests a multiphase crystallization in the glass. Under these considerations, each DSC crystallization peak was treated as a convolution of three individual peaks with distinct maxima temperature ( $T_p$ ). In order to evaluate the crystallization peaks as a function of temperature, the DSC curves were fitted using a computational least-square method considering three Gaussian functions with maxima temperatures  $T_{p1}$ ,  $T_{p2}$  and  $T_{p3}$ , as indicated in Fig. 2 (bottom inset). Figure 2 shows also a slight asymmetry observed on DSC crystallization peak at the smallest heating rate for all particle sizes glasses. This asymmetry suggests the existence of multiple crystalline phases during DSC scans. In this studied glass, the observed crystalline phases crystallizes at very close temperatures and on account of this a splitting of DSC crystallization peaks for small particle size was not clearly observed.

Table 1 summarizes the thermal properties of the studied glass as a function of different particle size and heating rates. As can be observed in this table, for particle size 45–63, 38–45 μm and smaller than 38 μm the  $T_g$  presents essentially the same values, if compared to the same heating rates. For particle

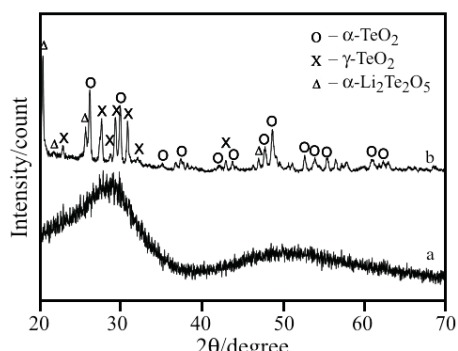


**Fig. 1** X-ray diffraction patterns of the as-quenched a –  $20\text{Li}_2\text{O}-80\text{TeO}_2$  glass and b – heat annealed at 642 K for 5 min

**Table 1** Summary for thermal parameters from DSC curves recorded for 20Li<sub>2</sub>O–80TeO<sub>2</sub> glass at different heating rates.

Particle size/ $\mu\text{m}$	$\phi/\text{K min}^{-1}$	Temperature/K						Energy/kJ mol <sup>-1</sup>		
		$T_g$	$T_x$	$T_{p1}$	$T_{p2}$	$T_{p3}$	$\chi^2$	$E_1$	$E_2$	$E_3$
63–75	2.5	537	596	600	605	610	0.0015			
	5.0	539	599	606	612	616	0.0065	296±3	298±1	327±1
	7.5	541	603	610	616	620	0.0017			
	10.0	542	605	614	619	623	0.0823			
45–63	2.5	533	594	599	603	607	0.0013			
	5.0	537	598	606	610	613	0.0071	292±1	296±1	324±1
	7.5	538	602	610	614	617	0.0146			
	10.0	540	604	613	617	620	0.1119			
38–45	2.5	535	593	595	600	604	0.0012			
	5.0	537	597	603	607	611	0.0077	255±2	293±1	297±1
	7.5	540	601	607	611	615	0.0384			
	10.0	542	602	611	614	618	0.0404			
<38	2.5	533	586	591	596	600	0.0004			
	5.0	537	589	600	603	607	0.0306	246±3	289±1	293±1
	7.5	537	592	604	607	611	0.0220			
	10.0	539	592	607	610	614	0.6092			

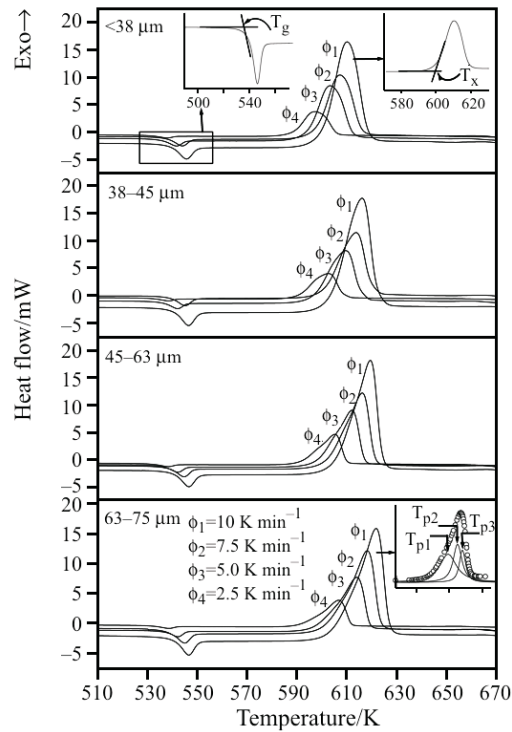
$T_g$ : the glass transition temperature,  $T_x$ : the crystallization temperature and  $T_{p1}$ ,  $T_{p2}$  and  $T_{p3}$ : temperatures at the maximum of the DSC crystallization peaks;  $\chi^2$ : refer to the fitting of DSC peaks by using three Gaussian functions (see text)

size 63–75  $\mu\text{m}$ , the  $T_g$  shifts to slightly higher temperatures. In same way,  $T_x$  shifts appreciably to lower values when particle size decreases. These variations may be associated with particle size effects on heat transfer during DSC scans, since larger particles would have greater heat transfer resistance when compared to small particles.

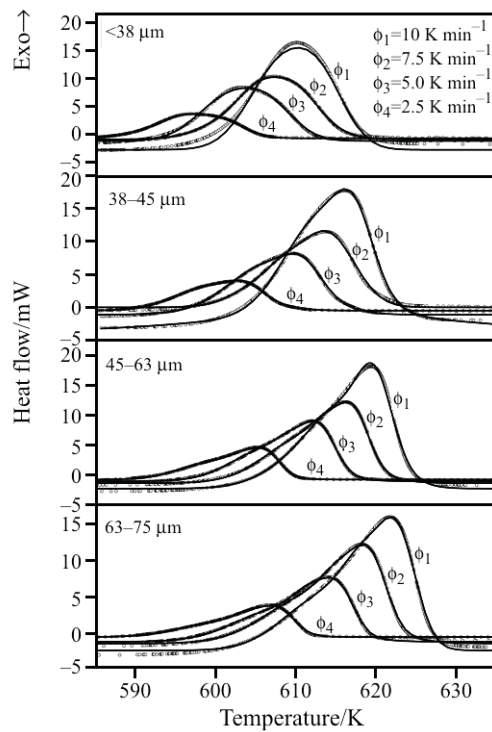
The activation energies  $E$  were determined for the three crystalline phases in the glass from the linear fitting of  $\ln(T_p^2 / \phi)$  vs.  $1/T_p$  plots by using the least-square method. The  $\chi^2$  values are usually used to attest the quality of a fit. The obtained  $\chi^2$  values ranged between  $1.00 \cdot 10^{-4}$  and  $7.74 \cdot 10^{-4}$ , indicating the good quality of these fittings. The results  $E_3 > E_2 > E_1$  ( $E_1 \approx E_2$ ) were also summarized in Table 1. The magnitude of activation energies obtained in this work is comparable to those reported in the literature for 30Li<sub>2</sub>O–70TeO<sub>2</sub> glass [3, 5]. Based on our previous results [22], the energies  $E_1$ ,  $E_2$  and  $E_3$  can be respectively associated to the following  $\gamma$ -TeO<sub>2</sub>,  $\alpha$ -TeO<sub>2</sub> and  $\alpha$ -Li<sub>2</sub>Te<sub>2</sub>O<sub>5</sub> crystallization in the 20Li<sub>2</sub>O–80TeO<sub>2</sub> glass.

Figure 3 shows experimental and theoretical re-constructed DSC crystallization peaks for 20Li<sub>2</sub>O–80TeO<sub>2</sub> glasses at different heating rates ( $\phi$ ) and different particle sizes. These fitting were carried out considering the maxima temperatures  $T_{p1}$ ,  $T_{p2}$  and  $T_{p3}$ , as summarized in Table 1. The  $\chi^2$  values obtained for each fitting were also summarized in Table 1. Except for the heating rate  $\phi=10^\circ\text{C min}^{-1}$ , that shows a relative high  $\chi^2$  values, the lower values obtained for  $\chi^2$  attest the good quality of these fittings. This result, associated to the XRD results, support the distinct three phases crystallization in the studied glass.

The crystallised volume fractions ( $x$ ), whose plots of  $x(T)$  shows a typical sigmoid type [23], was calculated for powdered glasses with particle size 63–75, 45–63, 38–45 and <38  $\mu\text{m}$ , considering each DSC deconvoluted crystallization peak, as



**Fig. 2** DSC curves of the 20Li<sub>2</sub>O–80TeO<sub>2</sub> glasses recorded at different heating rate ( $\phi$ ). Inset graphics indicates the onset glass transition temperature ( $T_g$ ), the onset crystallization temperature ( $T_x$ ) and temperatures at the maximum of the DSC crystallization peaks ( $T_{p1}$ ,  $T_{p2}$  and  $T_{p3}$ )



**Fig. 3** DSC crystallization peaks of the  $20\text{Li}_2\text{O}-80\text{TeO}_2$  glasses at different heating rates ( $\phi$ ) and particle sizes. Points represent experimental data and lines are the re-constructed theoretical result considering the maxima temperatures  $T_{p1}$ ,  $T_{p2}$  and  $T_{p3}$ , as shown in Table 1

shown in Fig. 2. The crystallized fraction ( $x$ ), at any temperature  $T$ , is given by  $x=A/A_0$  [24], where  $A_0$  is the total area between the temperature where the crystallization is just beginning ( $T_i$ ) and where the crystallization is completed ( $T_f$ ), and  $A$  is the area between

the initial temperature and a generic temperature  $T$ , located between  $T_i$  and  $T_f$ . The area  $A$  was determined by using a computer program with an algorithm based on Simpson's rule. Based on  $(dx/dt)$  vs. temperature plots, the maximum crystallization rates  $(dx/dt)_p$  were obtained and summarized in Table 2 for three crystallization peaks at different heating rates. Using these results and the activation energies summarized in Table 1, the Avrami exponent  $n$  were calculated and finally summarized in Table 2 for glasses with different particle size at different heating rates. The mean values  $\bar{n}$  obtained for glasses with different particle size were also summarized in Table 2. As we can see, distinct  $\bar{n}$  values were obtained for glasses with 63–75 and 45–63  $\mu\text{m}$  particle sizes such as  $\bar{n}_1 < \bar{n}_2 < \bar{n}_3$ , where  $\bar{n}_1 \approx 2.2$ ,  $\bar{n}_2 \approx 4.0$  and  $\bar{n}_3 \approx 5.5$ . However, glasses with particle size 38–45  $\mu\text{m}$  and smaller than 38  $\mu\text{m}$  shows  $\bar{n}_1 \approx \bar{n}_2 < \bar{n}_3$ , with  $\bar{n}_1 \approx 2.5$ ,  $\bar{n}_2 \approx 2.3$  and  $\bar{n}_3 \approx 5.5$ . The exponent  $n$  obtained in the present work is slightly greater than  $n=1.4$  obtained for  $30\text{Li}_2\text{O}-70\text{TeO}_2$  glasses [25].

The observed  $\bar{n}_1 < \bar{n}_2 < \bar{n}_3$  in the  $20\text{Li}_2\text{O}-80\text{TeO}_2$  glass is an indicative that nucleation and growth takes place by more than one mechanism in the early stages of the crystallization. The Avrami exponent  $n \approx 2$  indicates one-dimensional crystallization with a constant bulk nucleation rate,  $n \approx 3$  indicates the existence of the volume nucleation and the two-dimensional growth mechanism, while  $n \approx 4$  indicates volume nucleation and three-dimensional growth mechanism [26]. For  $n > 4$ , it is expected a three-dimensional crystallization with increasing nucleation rate followed by a controlled crystal growth. Thus, results show that the three deconvoluted crystallization peaks exhibit a distinct nucleation and growth for

**Table 2** Summary for maximum crystallization rate  $(dx/dt)_p$  and Avrami exponent ( $n$ ) for three crystallization peaks at different heating rates

Particle size/ $\mu\text{m}$	$\phi/\text{K min}^{-1}$	$dx_1/dt/\text{s}^{-1}$	$dx_2/dt/\text{s}^{-1}$	$dx_3/dt/\text{s}^{-1}$	$n_1$	$n_2$	$n_3$
63–75	2.5	0.00344	0.00630	0.00954	2.3	4.2	5.8
	5.0	0.00646	0.01167	0.01747	2.2	3.9	5.4
	7.5	0.00935	0.01691	0.02550	2.1	3.9	5.4
	10.0	0.01240	0.02279	0.03466	2.1	4.0	5.5
	$\bar{n}$				2.2	4.0	5.5
45–63	2.5	0.00374	0.00684	0.00980	2.5	4.5	5.9
	5.0	0.00731	0.01236	0.01779	2.5	4.2	5.6
	7.5	0.01041	0.01783	0.02606	2.4	4.1	5.5
	10.0	0.01391	0.02420	0.03605	2.4	4.2	5.8
	$\bar{n}$				2.4	4.2	5.7
38–45	2.5	0.00320	0.00383	0.00798	2.4	2.5	5.3
	5.0	0.00724	0.00724	0.01590	2.8	2.5	5.4
	7.5	0.00924	0.00924	0.02460	2.4	2.1	5.6
	10.0	0.01220	0.01220	0.03390	2.4	2.1	5.9
	$\bar{n}$				2.5	2.3	5.5
<38	2.5	0.00384	0.00463	0.00729	2.9	3.1	4.8
	5.0	0.00587	0.00922	0.01430	2.3	3.1	4.9
	7.5	0.00939	0.01370	0.02060	2.5	3.1	4.7
	10.0	0.01350	0.01680	0.02980	2.7	2.9	5.2
	$\bar{n}$				2.6	3.0	4.9

glasses with particle size 63–75 and 45–63 µm. Consequently, the increasing in  $\bar{n}$  exponent from  $n_1$  to  $n_3$  in these glasses suggests that growth mechanism changes from the initial one-dimensional crystallization with a constant nucleation to the three-dimensional crystal growth with nucleation rate increasing. On the other hand, for glasses with particle size 38–45 µm and smaller than 38 µm the both first and second deconvoluted crystallization peaks exhibit similar nucleation and crystal growth uni-dimensional while the third peak indicate a nucleation and three-dimensional growth mechanism.

## Conclusions

The crystallization of the 20Li<sub>2</sub>O–80TeO<sub>2</sub> glass was studied using XRD and DSC techniques to understand and control the crystallization kinetics on this glass matrix. XRD results show the  $\gamma$ -TeO<sub>2</sub>,  $\alpha$ -TeO<sub>2</sub> and  $\alpha$ -Li<sub>2</sub>Te<sub>2</sub>O<sub>5</sub> phase crystallization in the glass matrix. The measured activation energies showed that  $\gamma$ -TeO<sub>2</sub> and  $\alpha$ -TeO<sub>2</sub> crystallizes at very close temperatures but distinct for the  $\alpha$ -Li<sub>2</sub>Te<sub>2</sub>O<sub>5</sub> phase in this glass. From non-isothermal measurements was possible to see that no appreciable differences exists between  $n$  exponents for glasses with different particle sizes. Distinct  $\bar{n}$  values were obtained for glasses with 63–75 and 45–63 µm particle sizes such as  $\bar{n}_1 < \bar{n}_2 < \bar{n}_3$  while glasses with particle size 38–45 µm and smaller than 38 µm shows  $\bar{n}_1 \approx \bar{n}_2 < \bar{n}_3$ . The observed  $\bar{n}_1 < \bar{n}_2 < \bar{n}_3$  in the 20Li<sub>2</sub>O–80TeO<sub>2</sub> glass is an indicative that nucleation and growth takes place by more than one mechanism in the early stages of the crystallization.

## Acknowledgements

We would like to express our gratitude to Brazilian agencies CNPq, CAPES and FAPESP for their financial support.

## References

- 1 K. Tanaka, K. Kashima, K. Hirao, N. Soga, A. Mito and H. Nasu, *J. Non-Cryst. Solids*, 185 (1995) 123.
- 2 H. Nasu, O. Matsushita, K. Kamiya, H. Kobayashi and K. Kubodera, *J. Non-Cryst. Solids*, 124 (1990) 275.
- 3 I. Avramov, G. Guinev and A. C. M. Rodrigues, *J. Non-Cryst. Solids*, 271 (2000) 12.
- 4 T. Taniguchi, S. Inoue, T. Mitsuhashi and A. Nukai, *J. Appl. Cryst.*, 33 (2000) 64.
- 5 P. Balaya and C. S. Sunandana, *J. Non-Cryst. Solids*, 162 (1993) 253.
- 6 L. M. Tong, L. L. Hu, J. J. Zhang, J. R. Qiu, Q. Yang, J. Y. Lou, Y. H. Shen, J. L. He and Z. Z. Ye, *Optics Express*, 14 (2006) 82.
- 7 R. A. Montani, M. Lévy and J. L. Souquet, *J. Non-Cryst. Solids*, 149 (1992) 249.
- 8 A. Pan and A. Ghosh, *Phys. Rev. B*, 60 (1999) 3224.
- 9 J. Zhang, S. Dai, G. Wang, H. Sun, L. Zhang and L. Hu, *J. Lumin.*, 115 (2005) 45.
- 10 X. Feng, T. M. Monro, V. Finazzi, R. C. Moore, K. Frampton, P. Petropoulos and D. J. Richardson, *Electronics Lett.*, 41 (2005) 835.
- 11 R. El-Mallawany, *Mater. Chem. Phys.*, 53 (1998) 93.
- 12 R. El-Mallawany, *Mater. Chem. Phys.*, 60 (1999) 103.
- 13 W. A. Johnson and F. Mehl, *Trans. Amer. Inst. Mining Met. Engrs.*, 135 (1939) 416.
- 14 M. Avrami, *J. Chem. Phys.*, 7 (1939) 1103.
- 15 M. Avrami, *J. Chem. Phys.*, 8 (1940) 212.
- 16 H. E. Kissinger, *J. Res. Natl. Bur. Stand.*, 57 (1956) 217.
- 17 J. Vázquez, C. Wagner, P. Villares and R. Jiménez-Garay, *Acta Mater.*, 44 (1996) 4807.
- 18 J. Vázquez, P. L. López-Alemany, P. Villares and R. Jiménez-Garay, *Mater. Lett.*, 38 (1999) 423.
- 19 P. A. Thomas, *J. Phys. C: Solid State Phys.*, 21 (1988) 4611.
- 20 J. C. Champarnaud-Mersjard, S. Blanchandin, P. Thomas, A. Mirgorodsky, T. Merle-Mérjean and B. Frit, *J. Phys. Chem. Solids*, 61 (2000) 1499.
- 21 O. Noguera, T. Merle-Mérjean, A. P. Mirgorodsky, M. B. Smirnov, P. Thomas and J. C. Champarnaud-Mersjard, *J. Non-Cryst. Solids*, 330 (2003) 50.
- 22 E. Idalgo, E. B. Araújo, K. Yukimitu, J. C. S. Moraes, V. C. S. Reynoso and C. L. Carvalho, *Mater. Sci. Eng. A*, 434 (2006) 13.
- 23 C. Popescu, *Thermochim. Acta*, 285 (1996) 309.
- 24 A. Pratap, K. N. Lad, T. L. S. Rao, P. Majumdar and N. S. Saxena, *J. Non-Cryst. Solids*, 345 (2004) 178.
- 25 P. Balaya and C. S. Sunandana, *J. Non-Cryst. Solids*, 162 (1993) 253.
- 26 K. Matusita, T. Komatsu and R. Yokota, *J. Mater. Sci.*, 19 (1984) 291.

Received: August 13, 2007

Accepted: October 3, 2008

DOI: 10.1007/s10973-007-8683-6